

Broadband low-frequency resistive acoustic absorber via soft boundaries

Anis Maddi, Badreddine Assouar

▶ **To cite this version:**

Anis Maddi, Badreddine Assouar. Broadband low-frequency resistive acoustic absorber via soft boundaries. Physical Review Applied, 2026, 26 (1), pp.014106. ⟨10.1103/tgkv-cgrv⟩. ⟨hal-05773037⟩

HAL Id: hal-05773037

https://hal.science/hal-05773037v1

Submitted on 1 Oct 2026

HAL is a multi-disciplinary open access archive for the deposit and dissemination of scientific research documents, whether they are published or not. The documents may come from teaching and research institutions in France or abroad, or from public or private research centers.

L'archive ouverte pluridisciplinaire **HAL**, est destinée au dépôt et à la diffusion de documents scientifiques de niveau recherche, publiés ou non, émanant des établissements d'enseignement et de recherche français ou étrangers, des laboratoires publics ou privés.



Distributed under a Creative Commons CC BY 4.0 - Attribution - International License

Broadband low-frequency resistive acoustic absorber via soft boundaries

Anis Maddi[1,*] and Badreddine Assouar[1,†]

[1] *Université de Lorraine, CNRS, IJL, F-54000 Nancy, France*

(Dated: July 16, 2026)

Efficient sound absorption at low frequencies remains a major challenge, as most architectured materials rely on resonant mechanisms that limit their bandwidth. Here, we demonstrate a non-resonant approach based on resistive materials coupled to soft acoustic boundaries and show its effectiveness in different setups. In a reflection configuration, a critically coupled wire-mesh layer combined with a foam yields a high and broadband absorption over the investigated frequency range 10–6400 Hz. When considering a transmission configuration, placing a side hole near the wire-mesh layer breaks the mirror symmetry and results in a low-frequency and broadband one-sided absorption. This work opens new opportunities for acoustic materials by leveraging the potential of resistive materials for low frequency and broadband wave manipulation.

I. INTRODUCTION

In recent years, increasing attention has been devoted to the control of sound waves using engineered structures, largely motivated by advances in acoustic metamaterials. While a broad range of wave phenomena has been demonstrated using acoustic metamaterials, sound absorption [1–3] remains a central research topic due to its fundamental importance and relevance to industrial applications.

A major objective in sound absorption research is to achieve high absorption using minimally bulky structures. In this context, numerous studies have investigated various types of absorbers, including coiled structures, decorated membrane resonators (DMR), and Helmholtz resonators [4–16]. Although these approaches have demonstrated promising results, their implementation for low frequency absorption (below 100 Hz) remains challenging, since larger structures are needed. The minimal material thickness required to absorb a given bandwidth obeys the Kramers–Kronig relations [17]. Recent work has sought either to approach this limit or to circumvent it by breaking some of the fundamental assumptions underlying these relations, notably through the use of active systems [18–22].

Acoustic absorption problems can be broadly classified into two categories. The first, commonly referred to as the reflection problem, aims to suppress the reflected waves of a structure backed by a termination. This configuration is the most widely studied, and perfect absorption can be achieved at the resonance frequency when the acoustic impedance of the structure matches that of the surrounding medium, a condition known as critical coupling [23, 24]. The second category is the transmission problem, which concerns the absorption of a structure that can both reflect and transmit incident waves. This case is more challenging, as perfect absorption requires the simultaneous control of pressure and velocity discontinuities across the structure. Both problems have been investigated predominantly in the presence of hard-wall boundary conditions, which act either as a rigid backing in the reflection problem or as the confining duct in the transmission problem. This raises the question of how an absorbing structure behaves under soft boundaries, and whether such configurations can enable improved absorber designs. Here, the term soft boundary refers to a boundary condition where the waveguide is open to the surrounding medium through an opening.

Moving beyond hard-wall boundary conditions opens the possibility of revisiting classical absorption problems, notably the trade-off between thickness and bandwidth imposed by the conventional Kramers–Kronig relations. When soft boundaries are considered, the formulation of these relations differs fundamentally from that derived for rigidly backed systems [17, 25], thereby offering new perspectives for the design of sound absorbers. For instance, this allows pressure-drop induced systems, which in conventional rigid-backed setups would fail to absorb due to impedance mismatch. In particular, resistive materials are of significant interest in this context, as they do not rely on resonant mechanisms. One approach to implementing such systems involves the use of porous materials with capillary pores, such as wire-mesh layers, which can feature pore radii on the order of micrometers. Their use has been reported in a limited number of studies, including the realization of low frequency anechoic terminations [26, 27] and the design of absorbers [28–32].

In this work, we investigate the combined use of resistive materials and soft acoustic boundaries for superior sound absorption. We first demonstrate that a critically coupled wire-mesh layer of millimetric thickness achieves high acoustic absorption at low frequency (<100 Hz) when backed by a soft boundary in a reflection problem (see Fig.1.a). To broaden the absorption spectrum, an additional foam layer of thickness 4 cm is added. The resulting system suppresses reflected waves across a large frequency band ranging from 10 Hz to 6400 Hz (see Fig.1.b). Afterward, We consider the transmission configuration in which the same wire-mesh is positioned in the vicinity of a side-branch hole (see Fig.1.c-d). This new configuration leads to a strong low frequency and unidirectional absorption. In what follows, we will describe and analyze the different configurations and involved physical mechanisms for broadband acoustic absorption.

* anis.maddi@univ-lorraine.fr

† badreddine.assouar@univ-lorraine.fr

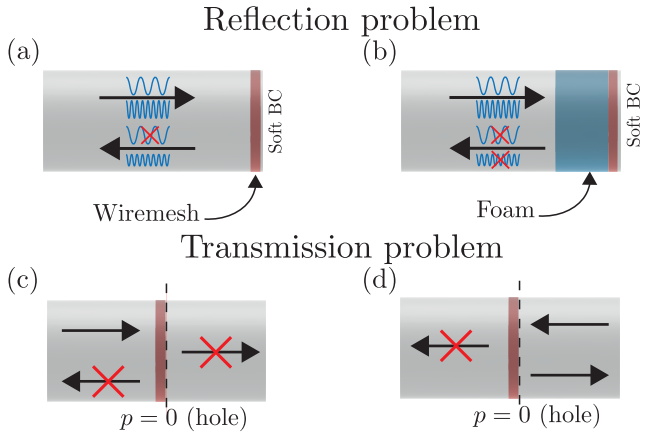


FIG. 1. **Absorption configurations using resistive materials.** (a–b) Reflection problem: a wire mesh layer is placed at the termination of a duct with soft boundary conditions. (a) When the wire mesh is critically coupled, it enables efficient absorption in the low-frequency range. (b) Adding a foam layer extends the absorption bandwidth by targeting higher frequencies. (c–d) Transmission problem: a side hole is introduced near the wire mesh. Waves incident from the left are absorbed (c), whereas waves incident from the right are predominantly reflected (d).

II. BACKGROUND

We consider a general acoustic scattering problem in which a linear scatterer placed in a waveguide is described by a transfer matrix $\mathbf{M}$, relating the acoustic pressure p and volume velocity u between the inlet and outlet,

$$\begin{pmatrix} p_2 \\ u_2 \end{pmatrix} = \underbrace{\begin{pmatrix} \mathbf{M}_{11} & \mathbf{M}_{12} \\ \mathbf{M}_{21} & \mathbf{M}_{22} \end{pmatrix}}_{\mathbf{M}} \begin{pmatrix} p_1 \\ u_1 \end{pmatrix}, \tag{1}$$

When the scatterer is placed at the extremity of a duct and rigid backing is assumed ($u_2 = 0$), the input impedance Z_{in} is given by

$$Z_{in}(\omega) = -\frac{\mathbf{M}_{22}}{\mathbf{M}_{21}}, \tag{2}$$

and the corresponding reflection coefficient reads

$$\mathscr{R}(\omega) = \frac{Z_c - Z_{in}}{Z_c + Z_{in}}. \tag{3}$$

where Z_c is the characteristic impedance of the waveguide.

Reflection problems have been widely investigated using various strategies to achieve the critical coupling condition $Z_c = Z_{\text{in}}$. Most existing realizations rely on resonant mechanisms to satisfy this condition, which inherently restricts their applicability at low frequencies. By contrast, non-resonant systems capable of providing broadband properties are particularly interesting, as they may enable impedance matching over a wide frequency range.

Wire-mesh layers provide a simple example of such a non-resonant resistive system. A layer of wire-mesh can be modeled as a network of parallel short capillary tubes. Acoustic wave propagation through this medium experiences a pressure drop proportional to a resistivity R_v. The corresponding transfer matrix can be written as [18]

$$\begin{pmatrix} p_2 \\ u_2 \end{pmatrix} = \begin{pmatrix} 1 & -R_v \\ 0 & 1 \end{pmatrix} \begin{pmatrix} p_1 \\ u_1 \end{pmatrix}. \tag{4}$$

The viscous resistance depends on the geometry of the capillary tubes (length ℓ, porosity ϕ, pore dimensions...) as well as on the properties of the propagating medium. For cylindrical pores, it is given by

$$R_v = \frac{8\eta\ell}{\phi\Lambda^2}, \tag{5}$$

where η is the dynamic viscosity of air. Note that this approximation assumes compactness (i.e. $k\ell \ll 1$) and that the pore radius is smaller than the viscous boundary layer thickness δ (i.e. $\Lambda \ll \delta$).

The broadband properties of wire-meshes make them particularly interesting for sound absorption. However, resistive materials introduce a pressure discontinuity, whereas critical coupling in rigid-backed configurations requires control of the velocity field at the termination. As a result, a resistive sheet alone cannot achieve impedance matching when backed by a rigid wall. This limitation can be overcome by assuming soft boundary conditions, where the termination enforces a null pressure condition ($p = 0$).

For instance, when the wire-mesh layer is placed at the extremity of a duct and a soft boundary is assumed (i.e. $p_2 = 0$ in Eq.1), the reflection coefficient is given by

$$r = \frac{Z_c - R_v}{Z_c + R_v}. \tag{6}$$

In the absence of radiation effects, perfect absorption (i.e. $r = 0$) is achieved under the critical coupling condition $R_v = Z_c$, which can be satisfied by appropriately tuning the wire-mesh geometry (see Eq.5). Since the resistivity is frequency independent (as far as the wire mesh is assumed compact), this configuration leads to broadband absorption. Note that in the limits of a very large or small geometrical parameter (e.g. radius Λ), $R_v \to 0$ or $R_v \to \infty$, the absorption performance is lost.

In practice, an ideal open boundary condition cannot be perfectly realized, and radiation effects must be taken into account, particularly at higher frequencies. Radiation introduces two main consequences. First, part of the acoustic energy is radiated outside the system. Second, the impedance-matching condition is modified, as the termination load is altered by the radiation impedance. For a circular duct of radius a, the radiation impedance Z_{rad} (baffle) can be approximated as

$$Z_{rad} = Z_c \left(\frac{(ka)^2}{2} + i\frac{8}{3\pi}ka \right), \tag{7}$$

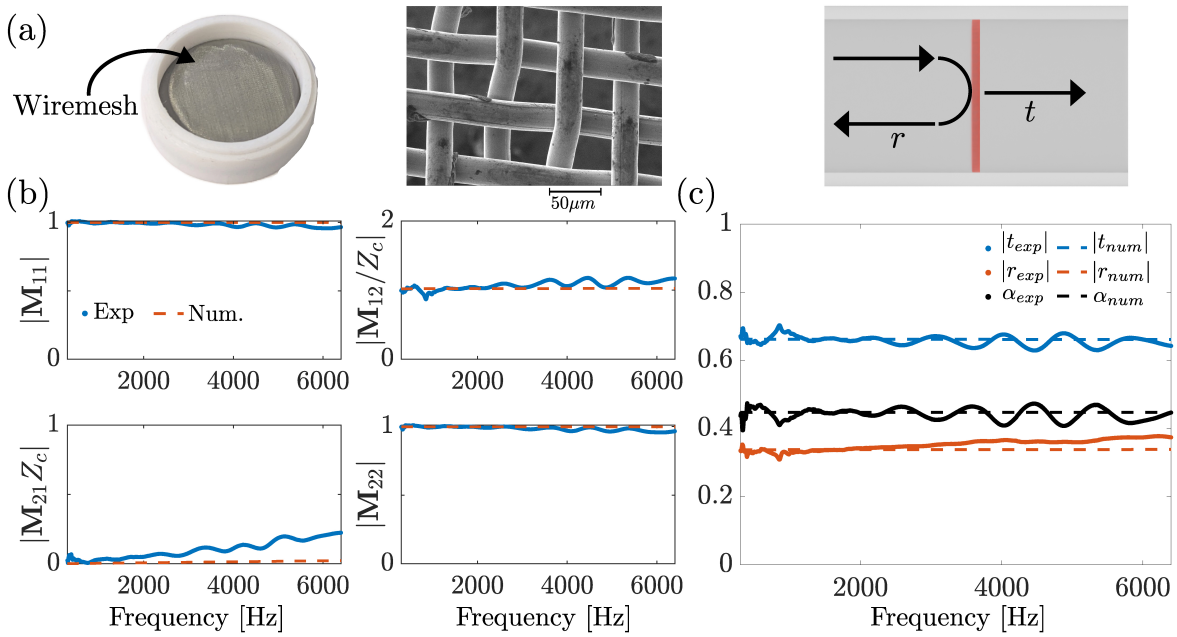


FIG. 2. Transfer and scattering coefficients of critically coupled wire mesh layers. (a) Picture of the wire-mesh layers and scanning electron microscopy (SEM) image showing the pore structure of one layer. (b) Normalized coefficients of the transfer matrix $\mathbf{M}$, where Z_c is the characteristic impedance of the duct. (c) Scattering coefficients, where r and t denote the reflection and transmission coefficients, respectively. Dots and dashed lines represent the experimental and numerical results obtained using a transfer-matrix approach.

where k is the acoustic wavenumber. The presence of this additional, frequency-dependent impedance alters the coupling condition and limits the achievable absorption, particularly at higher frequencies (i.e. $ka \gg 1$).

In this case, the reflection coefficient becomes

$$r = \frac{Z_c - R_v - Z_{rad}}{Z_c + R_v + Z_{rad}}. \tag{8}$$

Unlike conventional rigid-backed absorption problems, the presence of radiated power requires a refined definition of absorption. We therefore introduce two distinct quantities. The first is the anechoic (non-reflecting) coefficient, denoted by α_{anecho}, defined as

$$\alpha_{anecho} = 1 - |r|^2, \tag{9}$$

which quantifies the suppression of reflected waves inside the duct. A unitary value of α_{anecho} indicates complete elimination of reflected waves, i.e., an effectively anechoic termination from the duct perspective, but does not provide information about the acoustic power transferred to the exterior medium $\mathscr{P}_{rad}$. To account for the contribution of radiated waves, we define an absorption coefficient,

$$\alpha = 1 - |r|^2 - \frac{\mathscr{P}_{rad}}{\mathscr{P}_{inc}} \tag{10}$$

where $\mathscr{P}_{inc}$ denotes the incident acoustic power.

At low frequencies ($ka << 1$), the radiation impedance vanishes ($Z_{rad} \to 0$), and radiative losses are negligible. In this regime, the two coefficients coincide, and the absorption is dominated by viscous dissipation.

III. MATERIAL CHARACTERIZATION

The resistive material consists of a stack of 10 wire-mesh layers with an inner diameter of 25 mm. The wire-mesh was selected to have the smallest possible pore radius, which was estimated to be approximately 14 μm. Figure 2.(a) shows a photograph of the wire-mesh, along with a scanning electron microscopy (SEM) image that provides a view of the pore structure. The scattering and transfer coefficients are measured using a Brüel & Kjær impedance tube with an inner diameter of 29 mm. Two microphone spacings are used for our measurement: a standard spacing of 2 cm and a larger spacing of 24 cm to target lower frequencies.

Figure 2(b) displays the transfer-matrix coefficients obtained experimentally and numerically using a transfer-matrix approach. Good agreement is observed between these results, as well as with the theoretical prediction given in Eq. (4). Additionally, the wire-mesh used here is tuned such that the resistivity R_v (corresponding to the $\mathbf{M}_{1,2}$ term) matches the characteristic impedance Z_c, which corresponds to the critical coupling condition. This was performed experimentally by stacking multiple wire-mesh layers until the target value was reached.

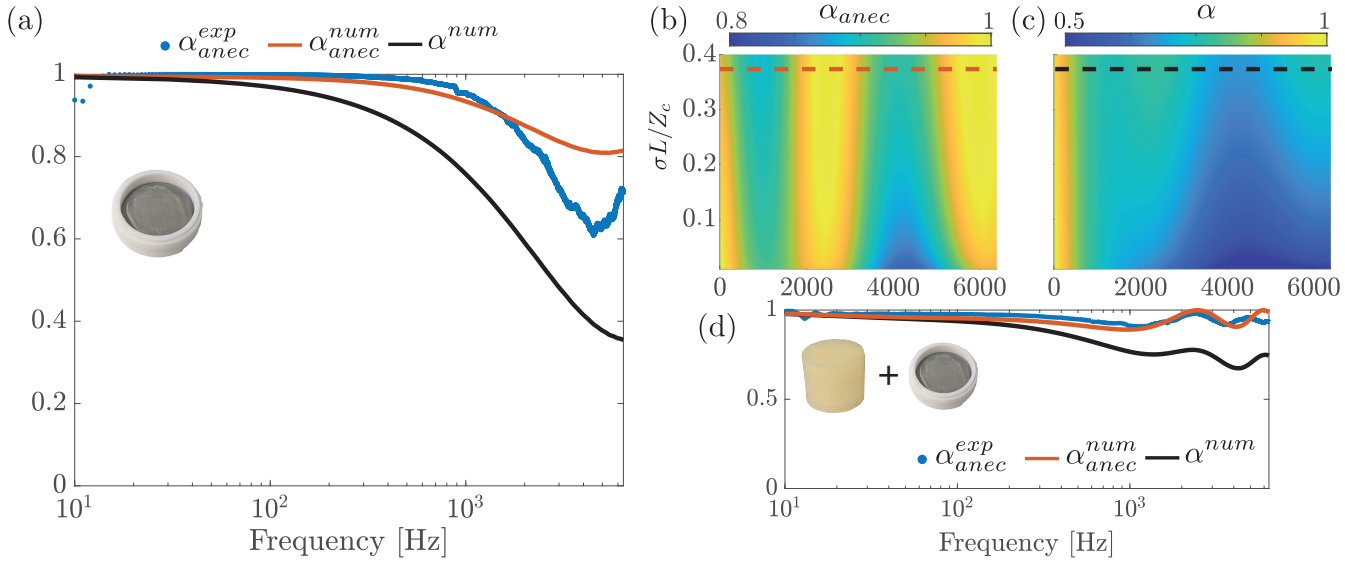


FIG. 3. **Anechoic and absorption properties of a wire-mesh layer with a soft boundary condition in a reflection problem.** (a) Anechoic coefficient α_{anec} obtained experimentally and numerically, together with the absorption coefficient α, shown in blue, red, and black, respectively. (b,c) Numerical simulations of the wire-mesh combined with a foam of length $L = 4$ cm. (b) Anechoic coefficient α_{anec}. (c) Absorption coefficient α. (d) Anechoic and absorption coefficients using the wire-mesh and a 4 cm of foam ($\sigma L/Z_c \approx 0.37$).

The reflection r, transmission t, and absorption coefficient α are shown in Figure 2(c), where good agreement between experimental and numerical results is also observed. Note that the absorption in such a two-port problem is fundamentally limited to 50% due to the mirror symmetry and compactness of the system. This limit can be overcome by breaking mirror symmetry [33] or using coherent perfect absorption [34].

Overall, the **M** and **S** coefficients demonstrate that the processes involved here are broadband over the investigated frequency range (up to 6.4 kHz) and that the impedance matching condition $R_v \approx Z_c$ is effectively achieved.

IV. REFLECTION PROBLEM

In this section, we consider a reflection problem in which a resistive material is placed at the end of an open duct. The numerical simulations presented here are performed using the COMSOL software. The wire-mesh is modeled as an impedance jump with a resistivity set to ρc. The absorption coefficient α is estimated numerically from the ratio between the power radiated and absorbed by the perfectly matched layer (PML), denoted by $\mathscr{P}_{\text{pml}}$, and the incident power at the duct inlet, $\mathscr{P}_{\text{inc}}$, such that

$$\alpha = 1 - |r|^2 - \frac{\mathscr{P}_{\text{pml}}}{\mathscr{P}_{\text{inc}}}. \tag{11}$$

As discussed in the previous section, the wire-mesh layer used here was optimized to achieve impedance matching (i.e., $R_v = Z_c$). The numerical and experimental results obtained by placing the wire-mesh at the end of a duct are shown in Figure 3(a). It is observed that the system behaves as a nearly perfect anechoic termination at low frequencies, down to 10 Hz. Note that this absorption is expected to remain high at lower frequencies. However, in practice, the measurements are limited experimentally by the microphone spacing.

As the frequency increases, the duct begins to radiate sound to the exterior medium, which also disrupts the impedance-matching condition. This, in turn, reduces the anechoic coefficient to 60% around 4 kHz in the experiments. The numerical simulations predict better suppression of reflected waves at higher frequencies compared to the measurements, which may be attributed to the compliance and inertance effects of the wire-mesh that were neglected in the numerical model. Additionally, when the power transmitted outside the duct is taken into account, a similar trend is observed: high absorption at low frequencies due to the limited radiated power, followed by a decrease in absorption down to approximately 35% around 6.4 kHz as the frequency increases.

These results indicate that the dominant mechanism at low frequencies is sound absorption induced by the resistive layers, whereas at higher frequencies, a significant contribution arises from acoustic energy radiating out of the duct. Importantly, the primary challenge in sound absorption typically lies in the low frequency regime. To enhance absorption at higher frequencies, a $L = 4$ cm thick foam slab (pore radii 200 μm) is placed in front of the wire-mesh (see [35] for its absorption coefficient) . The underlying idea is that the wire-mesh primarily suppresses low frequencies, while the foam absorbs the higher-frequency range.

Figures 3(b,c) present the numerical results obtained with the addition of a foam for varying normalized resistivity $\sigma L/Z_c$ and frequency. These results show that, as expected, introducing the foam significantly enhances both absorption and anechoicity at higher frequencies. The experimental results shown in Figure 3(d) confirm this trend and reveal a

substantial increase in the anechoic coefficient in the higher frequency regime. As a result, broadband anechoicity ranging from 90% to nearly 100% is achieved over a wide frequency band, ranging from 10 Hz to 6.4 kHz. This enhancement is induced by the additional absorption caused by the foam as highlighted by the numerical absorption coefficient α^{num}, which is greater than in the setup without foam (see Figure 3(a)).

V. TRANSMISSION PROBLEM

In this section, we consider a two-port scattering configuration in which a scatterer is placed inside a waveguide, allowing wave transmission from both sides. For a point-symmetric and reciprocal scatterer operating in the compact regime, the maximum achievable absorption under single-sided excitation is fundamentally limited to 50% of the incident acoustic power. Recent studies have proposed strategies to overcome this limit, notably by breaking mirror symmetry. Following this approach, we introduce a wire-mesh positioned in the vicinity of a side hole. This configuration breaks the mirror symmetry of the system and enforces an effective low frequency pressure-release condition ($p \approx 0$) near the wire-mesh.

Figure 4(a) shows a sketch and a picture of the system. The red line indicates the position of the wire-mesh, which is placed close to a side hole with a diameter of 10 mm (see [35] for details on the impact of the geometrical configuration). The wire-mesh used here is identical to that characterized previously. In the following, we are mostly interested in the low frequency regime where the radiation impedance is negligible.

The experimental results demonstrate that the reflection coefficients differ for the two directions of incidence, confirming the broken mirror symmetry. For waves incident from the left, the side hole is encountered first. At low frequencies, the side branch behaves approximately as a pressure-release termination, leading to strong reflection $|r^+| \approx 1$ (see Fig. 4(b)). In contrast, waves incident from the right first interact with the resistive material. The subsequent interference between the wire-mesh and the side hole results in simultaneously reduced reflection $|r^-|$ and transmission $|t|$. Consequently, at low frequencies, the system behaves as an absorber for right-incident waves and as a reflective boundary for left-incident waves. Note that the absorption is expected to remain high at lower frequencies, however, the frequency range is experimentally limited by the microphone spacing.

VI. CONCLUSION

While sound absorption remains an active area of research, most existing approaches focus on rigidly backed configurations and rely on resonant mechanisms to achieve impedance matching. In this work, we have demonstrated that combining resistive materials with open (soft) boundary conditions

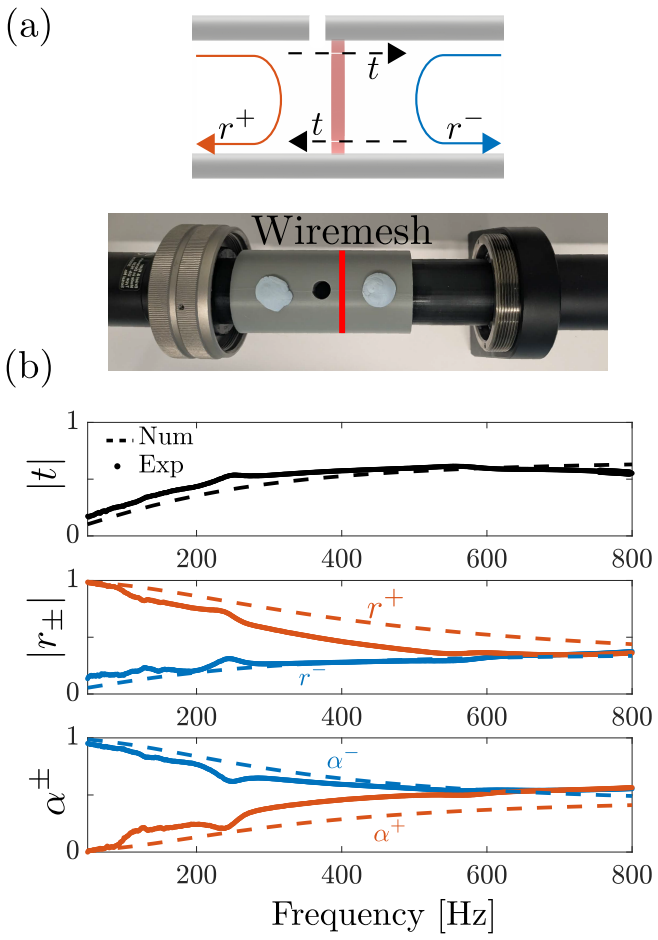


FIG. 4. **Low frequency absorption in a transmission problem.** (a) The wire-mesh is placed at the center of the duct, close to a side hole of diameter 1 cm. (b) The transmission t, reflection $r^\pm$ and absorption coefficient $\alpha^\pm = 1 - |t|^2 - |r^\pm|^2$ are displayed as function of frequency. Dots and dashed lines represent the experimental and numerical results.

provides a fundamentally different route to acoustic absorption. Building on the work of Dalmont et al. [26], we investigate configurations that combine resistive materials and open boundary conditions. We experimentally demonstrate that coupling a foam with a resistive wire-mesh under open boundary conditions yields a broadband anechoic termination operating down to the infrasound regime. We further examine the wire-mesh in a transmission configuration, where wire-mesh is inserted into a waveguide in the vicinity of a side hole. The results show that this system functions as a one-sided absorber, exhibiting strong low frequency absorption.

Beyond the specific implementation presented here, our results show that soft boundary conditions fundamentally modify the impedance-matching requirements of non-resonant absorbers. By relaxing the thickness constraints associated with rigid backing, this strategy opens new perspectives for the design of compact and broadband acoustic absorbers. Future work may explore the integration of metamaterials to further control radiation effects and improve sound mitigation.

ACKNOWLEDGMENTS

This work has been supported by l'Agence de l'Innovation de Défense (AID) in the context of the joint research laboratory MOLIERE, and by the IMPACT project LUE "I-META," part of the French PIA project "Lorraine Université d'Excellence" reference ANR-15- IDEX-04-LUE.

DATA AVAILABILITY

The data that support the findings of this study are available from the corresponding authors upon reasonable request.

REFERENCES

[1] N. Gao, Z. Zhang, J. Deng, X. Guo, B. Cheng, and H. Hou, Acoustic metamaterials for noise reduction: a review, Adv. Mater. Technol. **7**, 2100698 (2022).

[2] S. Qu and P. Sheng, Microwave and acoustic absorption metamaterials, Phys. Rev. Appl. **17**, 047001 (2022).

[3] M. Yang and P. Sheng, Sound absorption structures: From porous media to acoustic metamaterials, Annu. Rev. Mater. Res. **47**, 83 (2017).

[4] Y. Li and B. M. Assouar, Acoustic metasurface-based perfect absorber with deep subwavelength thickness, Appl. Phys. Lett. **108**, 063502 (2016).

[5] K. Donda, Y. Zhu, S.-W. Fan, L. Cao, Y. Li, and B. Assouar, Extreme low-frequency ultrathin acoustic absorbing metasurface, Appl. Phys. Lett. **115**, 173506 (2019).

[6] M. P. Abrahams, M. Oudich, Y. Revalor, N. Vukadinovic, and B. Assouar, Hybrid ultrathin metasurface for broadband sound absorption, Appl. Phys. Lett. **124**, 151702 (2024).

[7] H. Long, C. Shao, Y. Cheng, J. Tao, and X. Liu, High absorption asymmetry enabled by a deep-subwavelength ventilated sound absorber, Appl. Phys. Lett. **118**, 263502 (2021).

[8] F. Wu, Y. Xiao, D. Yu, H. Zhao, Y. Wang, and J. Wen, Low-frequency sound absorption of hybrid absorber based on micro-perforated panel and coiled-up channels, Appl. Phys. Lett. **114**, 151901 (2019).

[9] Y. Zhu, K. Donda, S. Fan, L. Cao, and B. Assouar, Broadband ultra-thin acoustic metasurface absorber with coiled structure, Appl. Phys. Express **12**, 114002 (2019).

[10] N. Jiménez, V. Romero-García, V. Pagneux, and J.-P. Groby, Rainbow-trapping absorbers: Broadband, perfect and asymmetric sound absorption by subwavelength panels for transmission problems, Sci. Rep. **7**, 13595 (2017).

[11] M. Yang, S. Chen, C. Fu, and P. Sheng, Optimal sound-absorbing structures, Mater. Horiz. **4**, 673 (2017).

[12] N. Wang, S. Huang, Z. Zhou, D. P. Tsai, J. Zhu, and Y. Li, Seven-octave ultrabroadband metamaterial absorbers via quality-factor-weighted mode density modulation, Natl. Sci. Rev. **12**, nwaf199 (2025).

[13] M. Yang, Y. Li, C. Meng, C. Fu, J. Mei, Z. Yang, and P. Sheng, Sound absorption by subwavelength membrane structures: A geometric perspective, Comptes Rendus Mécanique **343**, 635 (2015).

[14] S. Huang, X. Fang, X. Wang, B. Assouar, Q. Cheng, and Y. Li, Acoustic perfect absorbers via helmholtz resonators with embedded apertures, J. Acoust. Soc. Am. **145**, 254 (2019).

[15] Z. Zhou, S. Huang, D. Li, J. Zhu, and Y. Li, Broadband impedance modulation via non-local acoustic metamaterials, Natl. Sci. Rev. **9**, nwab171 (2022).

[16] G. Ma, M. Yang, S. Xiao, Z. Yang, and P. Sheng, Acoustic metasurface with hybrid resonances, Nat. Mater **13**, 873 (2014).

[17] S. Qu, M. Yang, S. Huang, S. Liu, E. Dong, H. Y. Li, P. Sheng, I. D. Abrahams, and N. X. Fang, Generalized causality constraint based on duality symmetry reveals untapped potential of sound absorption, Nat. Commun. **16**, 10749 (2025).

[18] A. Maddi, C. Olivier, G. Poignand, G. Penelet, V. Pagneux, and Y. Aurégan, Frozen sound: An ultra-low frequency and ultra-broadband non-reciprocal acoustic absorber, Nat. Commun. **14**, 4028 (2023).

[19] S. Sergeev, R. Fleury, and H. Lissek, Ultrabroadband sound control with deep-subwavelength plasmacoustic metalayers, Nat. Commun. **14**, 2874 (2023).

[20] E. Rivet, S. Karkar, and H. Lissek, Broadband low-frequency electroacoustic absorbers through hybrid sensor-/shunt-based impedance control, EEE Trans. Control. Syst. **25**, 63 (2016).

[21] H. Lissek, R. Boulandet, and R. Fleury, Electroacoustic absorbers: bridging the gap between shunt loudspeakers and active sound absorption, J. Acoust. Soc. Am. **129**, 2968 (2011).

[22] X. Guo, H. Lissek, and R. Fleury, Improving sound absorption through nonlinear active electroacoustic resonators, Phys. Rev. Appl. **13**, 014018 (2020).

[23] A. Maddi, G. Poignand, V. Achilleos, V. Pagneux, and G. Penelet, Direct experimental observation of total absorption and loss compensation using sound waves with complex frequencies, J. Appl. Phys. **137** (2025).

[24] V. Romero-García, G. Theocharis, O. Richoux, A. Merkel, V. Tournat, and V. Pagneux, Perfect and broadband acoustic absorption by critically coupled sub-wavelength resonators, Sci. Rep. **6**, 19519 (2016).

[25] Y. Meng, V. Romero-García, G. Gabard, J.-P. Groby, C. Bricault, S. Goudé, and P. Sheng, Fundamental constraints on broadband passive acoustic treatments in unidimensional scattering problems, Proceedings of the Royal Society A **478**, 20220287 (2022).

[26] J. Dalmont, J. Kergomard, and X. Meynial, Realization of an anechoic termination for sound ducts at low-frequencies, C. R. Acad. Sci. Paris **309**, 453 (1989).

[27] F. Fohr and E. Portier, Conduit comprenant au moins une terminaison anéchoïque comprenant un moyen d'absorption acoustique basses fréquences et un moyen d'absorption acoustique moyennes et hautes fréquences, French Patent No. FR 3 074 556 B1 (2021), filed December 5, 2017.

[28] Y. Aurégan, Ultra-thin low frequency perfect sound absorber with high ratio of active area, Appl. Phys. Lett. **113**, 201904 (2018).

[29] H. Y. Mak, X. Zhang, Z. Dong, S. Miura, T. Iwata, and P. Sheng, Going beyond the causal limit in acoustic absorption, Phys. Rev. Appl. **16**, 044062 (2021).

[30] C. Ge, N. Wang, X. Wang, and Y. Li, Causal-constraint broadband sound absorption under isothermal process, Phys. Rev. Lett. s **134**, 237001 (2025).

[31] Y. Zhu, Z. Tao, J. Zhang, H. Long, T. Wang, J. Qin, Y. Cheng, and X. Liu, Ultrabroadband sound absorption enabled by a hybridized soft boundary, Phys. Rev. Appl. **25**, 014036 (2026).

[32] Y. Zhu, C. Gong, X. Zhang, H. Long, T. Wang, Y. Cheng, and X. Liu, An ultrathin absorber for broadband low-frequency sound enabled by an impedance boundary, App. Phys. Lett. **126**, 251702 (2025).

[33] A. Merkel, G. Theocharis, O. Richoux, V. Romero-García, and V. Pagneux, Control of acoustic absorption in one-dimensional scattering by resonant scatterers, Appl. Phys. Lett. **107**, 244102 (2015)M. Farooqui, Y. Aurégan, and V. Pagneux, Ultrathin resistive sheets for broadband coherent absorption and symmetrization of acoustic waves, Phys. Rev. Appl. **18**, 014007 (2022).

[34] A. Maddi, M. Oudich, A. Merkel, J. A. I. Martínez, and B. Assouar, Acoustic scattering singularities via quasi-bound states in the continuum, arXiv preprint arXiv:2512.16672 (2025).

[35] See Supplemental Material at [URL will be inserted by publisher] for details on the impact of the geometrical configuration and absorption properties.